






Impact of Fabrication and Testing Parameters on the Performance of a Polymer Electrolyte Fuel Cell with Platinum Group Metal (PGM)-Free Cathode Catalyst

Luigi Osmieri,^{*,*}  Hao Wang,^{*,*}  and Kenneth C. Neyerlin^z 

National Renewable Energy Laboratory, Golden, Colorado 80401, United States of America

Extensive research efforts have been made on platinum group metal (PGM)-free electrocatalysts for oxygen reduction reaction, with the aim of lowering the cost hurdle of acidic polymer electrolyte fuel cells (PEFCs). While the activity and durability of PGM-free catalysts have been boosted, the PEFC performance relies also on the electrode structure at the membrane electrode assembly (MEA) level. However, the extensive number of variables involved in the electrode preparation as well as in the fuel cell testing, poses severe challenge to compare results obtained in different labs. In this work, we systematically investigated the effect on performance of some operational variables, such as polarization curve scan direction, and gas flow rates. Additionally, anodic Pt catalyst loading and cathodic PGM-free catalyst loading were investigated. The tests were done in a differential cell hardware using a commercial Fe-N-C catalyst at the cathode. The results indicate that PGM-free catalyst loading and air flow rate on the cathode are impactful variables. Polarization curve scan direction (also considering averaging process on multiple consecutive scans), anode Pt loading as low as 0.035 mg cm⁻², as well as H₂ and O₂ flow rates above 300 scm³ min⁻¹ have negligible impact on the performance of PGM-free based MEAs.

© 2021 The Author(s). Published on behalf of The Electrochemical Society by IOP Publishing Limited. This is an open access article distributed under the terms of the Creative Commons Attribution 4.0 License (CC BY, <http://creativecommons.org/licenses/by/4.0/>), which permits unrestricted reuse of the work in any medium, provided the original work is properly cited. [DOI: 10.1149/1945-7111/abd48e]



Manuscript submitted August 20, 2020; revised manuscript received October 19, 2020. Published January 7, 2021.

Supplementary material for this article is available [online](#)

Polymer electrolyte fuel cell (PEFC) devices enable to efficiently convert the chemical energy of a fuel and an oxidant through electrochemical reactions.¹ If produced using renewable energy sources, H₂ represents an emission-free fuel that can be utilized in PEFCs.^{2,3} Great progresses have been achieved in recent years on acidic PEFC performance and durability, in parallel with the reduction of precious metal loadings, enabling the commercialization of vehicles powered by PEFC stack devices.^{4,5} However, the use of Pt as preferred catalyst for both H₂ oxidation reaction (HOR) and O₂ reduction reaction (ORR) remains prominent.^{6,7} Pt is a costly noble metal which might suffer supply issues in a scenario of PEFC devices manufacturing on a large-scale.^{8,9} Due to the sluggish kinetics of the ORR compared to the HOR, most of the Pt loading in a PEFC is needed at the cathode.^{10,11} For this reason, relevant efforts have been made in developing ORR electrocatalysts free of noble metals, often named Platinum Group Metal (PGM)-free catalysts.^{12,13} Carbon-based materials containing N and transition metals (e.g. Fe, Co, Mn) dopants have been demonstrated to be the most promising class of PGM-free catalysts in terms of activity and durability. These materials are denoted as M-N-C catalysts, where M stands for the active transition metal.^{14–17}

Along with an extensive number of works about synthesis, characterization, and test in three-electrode cells, research has started to focus on the integration of such catalysts in operating electrodes at the membrane electrolyte assembly (MEA) level.^{18–21} M-N-C catalysts have a lower intrinsic mass activity compared to the Pt/C benchmark catalysts, which is ascribed to their lower active site density and turnover frequency.^{18,22} Consequently, to achieve acceptable PEFC performance, the PGM-free catalyst loading on the cathode must be higher than for a regular Pt/C catalyst, resulting in ca. 10 times thicker cathode catalyst layer (CCL), i.e. 10 μm vs 100 μm.^{23,24} Having an order of magnitude thicker CCL causes a considerable increase in transport resistance of the ORR reactants: the O₂ gas through the electrode pores, and the H⁺ ions through the ionomer.^{25,26} Both resistances are related to the length, narrowness, and tortuosity of their paths towards the catalyst active sites.^{27–30}

Therefore, a thick CCL clearly becomes a major source of mass transport and ohmic (ionic) overpotentials during fuel cell operation.²⁴

Recently, extremely promising performances in acidic PEFC have been achieved for M-N-C catalysts, demonstrating the excellent work carried out in this field by different research groups.^{19,31–34} As much as the research achievements make step forward, it is necessary to uniform the PEFC testing conditions across the scientific community to report comparable results. This has been done more extensively for PEFC containing Pt/C catalysts, where specific testing protocols have been established by different institutions.^{35,36} Using the same testing conditions would enable a fairer performance comparison between different PGM-free electrocatalysts at MEA level. Unfortunately, the testing and the MEA fabrication variables are numerous, as summarized in Table I, making the comparison of results obtained by different research groups more difficult.

The aim of this study is to better understand the effects on the performance of a PGM-free-based MEA of some of these variables that have not been systematically explored thus far.

In this study, we investigated two MEA fabrication variables: the Pt catalyst loading on the anode and the PGM-free catalyst loading on the cathode.

It is a common belief that the Pt loading on the anode does not have any impact on the performance of an acidic PEFC, due to the significantly low kinetic overpotential of the HOR compared to the ORR. This was demonstrated for MEAs containing Pt/C catalysts at the cathode,^{37,38} but there is not any explicit report for MEAs with PGM-free cathode catalysts.

As far as the impact of cathode catalyst loading is concerned, several works about Pt/C MEAs, have shown that it is a key variable to dictate the PEFC performance.^{39–43} The impact of the Pt loading on the cathode is evident at both low and high current densities. At low current density, the sluggish ORR kinetics is the major source of overpotential, and having a higher Pt loading increases the electrochemically active surface area.⁴³ At high current density, the so called local O₂ resistance at the interface between ionomer and Pt surface becomes higher for low Pt loadings, increasing the mass transport overpotential.⁴⁴ Technical advancements on catalysts and electrode structures have recently led to obtain outstanding performances even with Pt loadings on the cathode as low as

[†]These authors contributed equally to the work.

*Electrochemical Society Member.

^zE-mail: kenneth.neyerlin@nrel.gov

Table I. List of variables that may have an impact on PEFC performance.

Type	Variable
MEA fabrication	Anode catalyst loading
	Anode ionomer-to-catalyst (I/C) ratio
	Ink deposition method (e.g. hand painting, spray coating, roll-to-roll coating)
	Ink processing (e.g. mixing/dispersion mode, time, power)
	Ink composition (solvents, solid concentration)
	Ink deposition substrate (membrane, diffusion media)
	Ionomer (chemistry, equivalent weight)
	Cathode catalyst loading
	Cathode ionomer-to-catalyst (I/C) ratio
	MEA hot pressing (time, temperature, pressure)
	Membrane (thickness, ionomer chemistry, mechanical reinforcement, chemical stabilizer)
Cell assembly	Diffusion media type
	Gasket thickness (electrodes compression)
Testing	Flow field geometry
	Temperature
	Pressure
	Relative humidity
	Gas flow rate
	Gas flow direction (co-flow, counter-flow)
	Polarization curve scan direction
	Polarization curve steps number and duration
	MEA conditioning

0.06 mg cm⁻².⁶ For PGM-free catalysts, the literature reporting on the effect of cathode catalyst loading on the performance is not so abundant. Some pioneering studies were published about H₂ and direct methanol fuel cells, but a clear loading vs performance trend was not always observed, and the performance was also influenced by the ionomer content in the CCL.^{45–49} Even though a systematic study has not been reported so far, a recent review pointed out that in the majority of the works about PGM-free catalysts tested in acidic PEFC the cathode catalyst loading is 4 mg cm⁻².¹⁵ More recently, modeling efforts based on experimental results of PEFC prepared with a Fe–N–C catalyst, have shown the prediction of the beneficial effects of higher catalyst loadings in the low current density region, and of lower catalyst loadings in the high current density region.²⁴

We also investigated the effect of two testing variables: the polarization curve scan direction, and the gas flow rate (on both anode and cathode).

For Pt-based catalysts in both liquid electrolyte cell (e.g., rotating disk electrode, RDE) and MEA, the ORR activity is better when the polarization curve is measured in the anodic scan direction. This is due to the well-known potential dependent Pt oxide coverage effect.^{43,50–52} For M–N–C catalysts instead, in both RDE and MEA, the polarization curves are usually measured in the cathodic scan direction. However, to the best of our knowledge, there is no evidence in the literature that such a comparison was made.

By analyzing the experimental sections of many papers reporting on PGM-free catalysts testing at the MEA level, we can see that in most of the cases the polarization curves are measured using a fixed gas flow rate on both anode and cathode. To the best of our knowledge, a systematic investigation of the gas flow rates impact on the performance of PGM-free based PEFC is not reported in the literature. However, some literature exists about Pt catalysts in H₂-fueled PEFCs for single cells⁴¹ and stacks,⁵³ and also in direct methanol fuel cells.⁵⁴ All these studies show a beneficial effect of increasing the cathode air flow rate at high current densities, well explicable with increasing stoichiometry, as also confirmed by modeling results.⁵⁵

It is well recognized in the literature that PGM-free catalysts suffer durability issues.^{56,57} This means that even the measurement of a few polarization curves, or the operation under steady state for a relatively short time, might significantly alter the results obtained. Thus, to better quantify this effect, in this work we also evaluated the

degradation due to the measurement of 6 consecutive polarization curves.

Through a systematic investigation we demonstrated that the impacts on the MEA performance in a 5 cm² differential cell hardware of the Pt catalyst loading and the gas flow rate on the anode are negligible. On the other hand, we demonstrated that the PEFC performance largely depends on the PGM-free catalyst loading and the air flow rate on the cathode. Additionally, the O₂ gas flow rate in the range investigated does not influence the performance, as well as the polarization curve scan direction.

Materials and Methods

MEA preparation.—The process of the MEAs fabrication was well established and documented in previous publications,^{24,58} and it is schematized in Fig. 1a. First, the anode gas diffusion electrode (GDE) was prepared by dispersing a Pt/C catalyst (50 wt% Pt on Vulcan, TEC10V50E, TKK) in a mixture of deionized (DI) water and n-propanol (volume ratio 4:3) and Nafion ionomer solution (DE2020, Ion Power) to achieve a solid concentration of ~2 mg ml⁻¹ and an ionomer to carbon ratio (I/C) of 0.6. The ink was tip-sonicated for 20 s and then for 20 min in an ice bath. Then the ink was sprayed using an automatic ultrasonic spray coating system (Sono-Tek) on the top of a 5 cm² piece of Sigracet SG29BC carbon paper gas diffusion layer (GDL). Three types of anode GDEs were prepared, having different Pt loadings of 0.2–0.1–0.035 mg cm⁻². The Pt loading was measured by X-ray fluorescence spectroscopy (XRF) with a Fischer FISCHERSCOPE[®] X-ray XDV[®]-SDD instrument.

The cathode catalyst ink was prepared by mixing the Fe–N–C catalyst (PMF-011904, Pajarito Powder LLC) with a solution of isopropanol and DI water (1:1 wt. ratio) and Nafion ionomer solution (LIQUION LQ-1105, Ion Power) to achieve a solid concentration of ~26 mg ml⁻¹ and a ionomer content in the dry electrode of 35 wt%. Then, ink was sonicated for 3 h in an ice bath.

The anode GDE was hot pressed at 120 °C for 5 min at 4 MPa on a piece of Nafion N211 membrane to obtain a half-MEA. Then the half-MEA was placed on a vacuum-sealed porous plate heated at 95 °C with the anode GDE in contact with the plate and the cathode catalyst ink was deposited on the upper side of the membrane using a paint brush. MEAs with three different cathode catalyst loadings

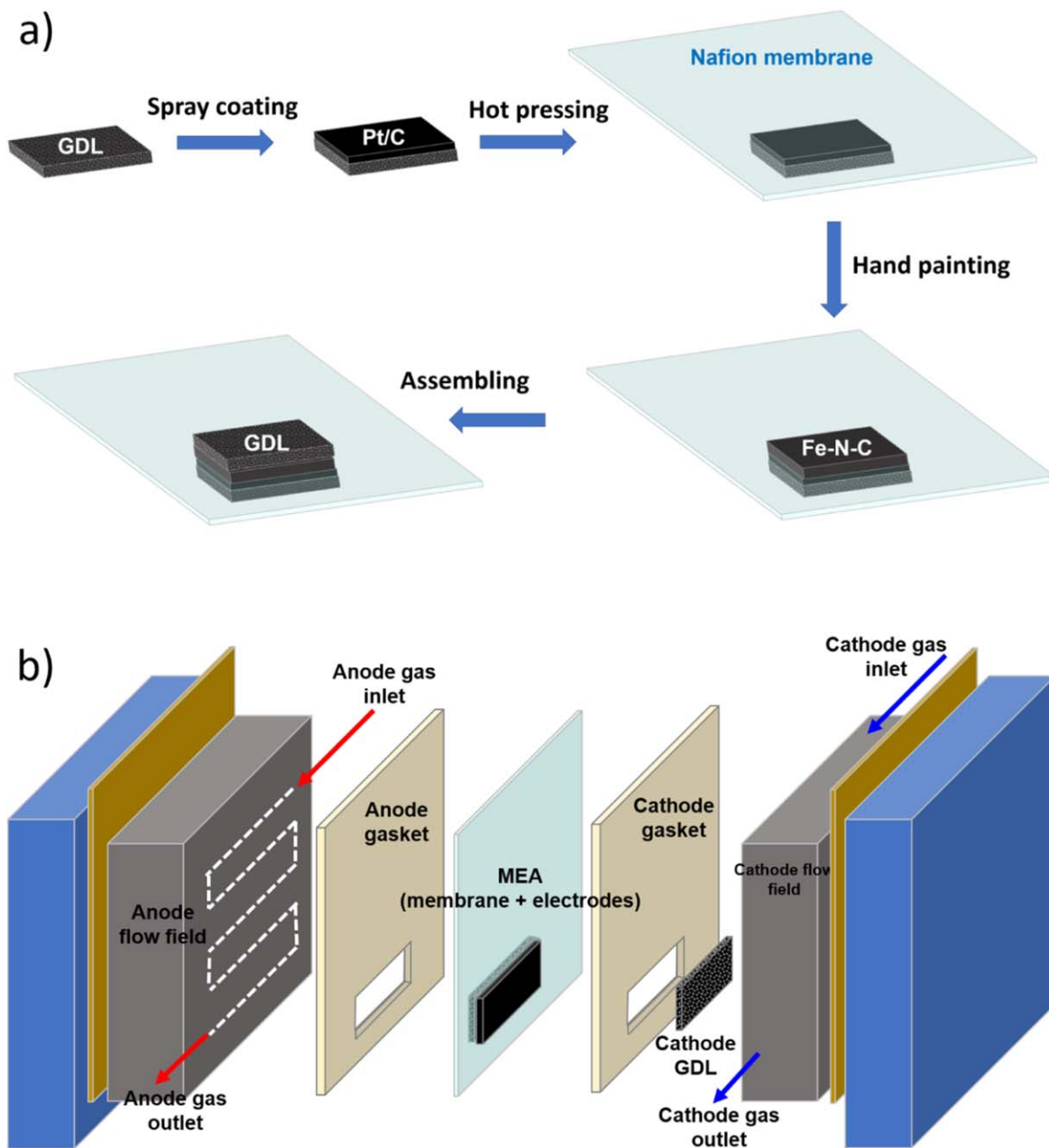


Figure 1. (a) Schematic of the MEA fabrication process. (b) Illustration of the MEA assembly in the fuel cell hardware.

(2–4–6 mg cm⁻²) were prepared. The cathode catalyst loading was verified by measuring the thickness of the catalyst layer deposited, assuming a packing density of 0.4 g cm⁻³.²³ Table II summarizes all

the MEAs that were prepared. The MEAs of *Series 1* were used to test the impact of the anode Pt loading and the polarization curve scan direction. The MEAs of *Series 2* were used to test the impact of

Table II. List of the MEAs fabricated for the experiments carried out in this work.

MEA#	Anode catalyst loading (mg cm ⁻²)	Cathode catalyst loading (mg cm ⁻²)	Experiment series
1	0.2	4	BOT Reproducibility
2	0.2	4	BOT Reproducibility
3	0.2	4	BOT Reproducibility/Series 1
4	0.1	4	Series 1
5	0.035	4	Series 1
6	0.2	2	Series 2
7	0.2	4	Series 2
8	0.2	6	Series 2
9	0.2	4	Series 3

Table III. Test protocol for the Series I experiments: effect of anode Pt loading and polarization curve scan direction. All the polarization curves were measured at 80 °C, 150 kPa, and 100% RH, with anode and cathode gas flow rate of 1000 $\text{scm}^{-3} \text{min}^{-1}$.

Order	Polarization curve type	Scan Direction	Notes
1	H ₂ /air	Cathodic	Control BOT air
2	H ₂ /air	Anodic	Control BOT air
3	H ₂ /O ₂	Cathodic	Control BOT O ₂
4	H ₂ /O ₂	Anodic	Control BOT O ₂
5	H ₂ /air	Cathodic	6 repeats air
6	H ₂ /air	Anodic	
7	H ₂ /air	Cathodic	
8	H ₂ /air	Anodic	
9	H ₂ /air	Cathodic	
10	H ₂ /air	Anodic	
11	H ₂ /O ₂	Cathodic	6 repeats O ₂
12	H ₂ /O ₂	Anodic	
13	H ₂ /O ₂	Cathodic	
14	H ₂ /O ₂	Anodic	
15	H ₂ /O ₂	Cathodic	
16	H ₂ /O ₂	Anodic	
17	H ₂ /air	Cathodic	Control EOT air
18	H ₂ /air	Anodic	Control EOT air

the cathode catalyst loading and the anode and cathode simultaneous flow rate variation. The MEA of Series 3 was used to test the effects of independent gas flow rate variation on anode and cathode.

MEA testing.—The MEA was assembled in the fuel cell hardware as illustrated in Fig. 1b. Two PTFE gaskets were placed respectively on the anode and cathode side of the MEA. The total thickness of the gaskets was selected according to the electrodes thickness, to have a diffusion media compression of 20%. A piece of Sigracet SG29BC GDL was placed on the top of the CCL. A graphite flow field with differential cell geometry was used, as described in previous works.^{24,30} The electrodes are placed on a straight portion of the flow field close to the gas outlet manifold, where the cell pressure is measured. With this configuration, a negligible pressure drop occurs across the MEA active area section.

The polarization curves were recorded using a fully automated Hydrogenics fuel cell test station. Prior to start the test, the cell was heated up to 60 °C flowing N₂ at ambient pressure on both anode and cathode. Then the anode gas flow was switched to H₂, the cell temperature was increased to 80 °C, the pressure was set to 150 kPa (absolute), and the relative humidity was set to 100% on both anode

and cathode, and after ca. 20 min the cathode gas flow was switched from N₂ to air. All the polarization curves were measured at 80 °C, 150 kPa, and 100% RH. The polarization curves were measured in voltage control mode, in the conditions and order described in Tables III–V, varying depending on the test series. The voltage steps were of 25 mV from OCV to 0.7 V, 50 mV from 0.7 to 0.4 V, and 100 mV from 0.4 to 0.1 V. For each step, the hold time was 75 s, and the current density was averaged on the last 60 s. The high-frequency resistance (HFR) was measured on-line during the polarization curve scan at 6000 Hz frequency.

Results and Discussion

MEA performance reproducibility.—As a first step of this work, we wanted to verify the reproducibility of the polarization curves results. This is an important aspect, especially considering that the MEA fabrication involves a hand-painting process for the cathode catalyst layer. Even though we had previously validated the reproducibility of this MEA fabrication method with other PGM-free catalysts,^{24,58–60} we wanted to have a further confirmation of its goodness also for this commercial Fe–N–C material. To do this, we fabricated three identical MEAs (MEAs #1–2–3, see Table II), and we compared the beginning of test (BOT) polarization curves measured in standard conditions (or baseline conditions), that is, at 80 °C, 150 kPa, and 100% RH. According to Table II, throughout this work, we prepared two additional MEAs (#7 and #9) with the same characteristics. With a total of five MEAs, a reliable indication can be obtained about reproducibility. Figure 2a shows the polarization curves measured at BOT for MEAs #1–2–3–7–9. The average is also plotted, with error bars representing the standard deviation.

Figure 2a also shows the HFR values measured with each point of the polarization curve. The HFR represents the sum of the ionic resistance of the membrane, and the electronic resistance of the electrodes, diffusion media, and cell hardware such as flow field plates, current collectors, and cables. Figure 2b shows the polarization curves corrected for the HFR contribution on a semi-logarithmic plot, enabling a better visualization of the low current density region. With these data we demonstrated that a good reproducibility was obtained for this MEA fabrication method and with this specific Fe–N–C catalyst. Thus, we could move forward with investigating the effect of the fabrication and testing parameters on the PEFC performance with a good confidence.

The performance of these PGM-free MEAs is still low compared to Pt/C MEAs prepared fabricated in our lab.^{61–63}

Effects of anode Pt loading.—The impact of the anode catalyst loading on the performance of PEFCs fabricated using PGM-free catalysts at the cathode has not been demonstrated in the literature to

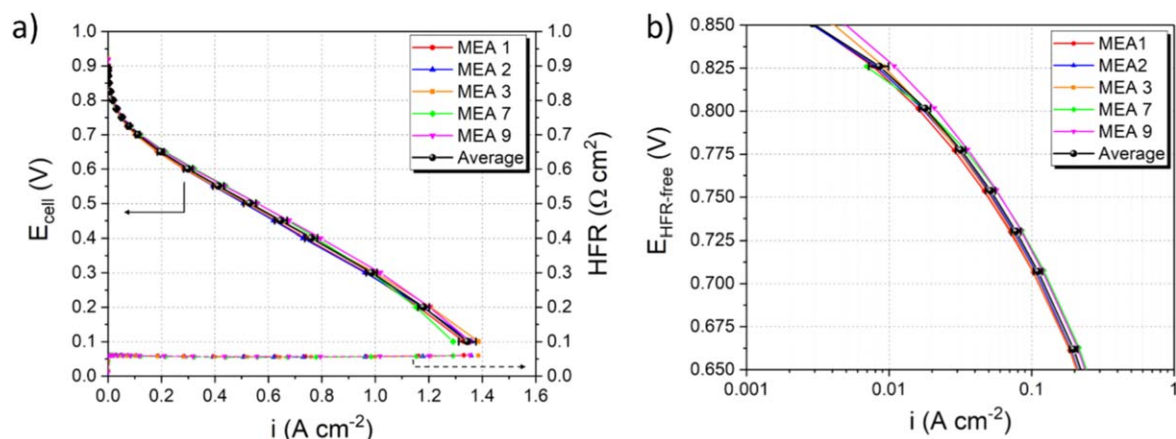


Figure 2. (a) Beginning of test H₂/air polarization curves (left axis) and HFR (right axis) measured at 80 °C, 150 kPa, and 100% RH for the 5 MEAs fabricated in the same way. (b) Detail of the low current density region of the polarization curves in (a) corrected for the HFR contribution. Error bars represent the standard deviation of the 5 MEAs.

date. A publication by Gasteiger et al. showed that for a Pt/C based MEA, reducing the anode Pt loading from 0.4 to 0.05 mg cm⁻² causes a voltage loss of less than 10 mV at ca. 1 A cm⁻².³⁸ A PGM-free CCL has a more limited ORR performance than a Pt/C one, due to the lower active site density, and to the higher proton and gas mass transport resistances caused by the higher thickness.¹⁰ Thus, the influence of the anode on the overall cell performance should be lower for a PGM-free based MEA than for a Pt/C one. However, this aspect deserves to be investigated to clarify doubts, since there is no evidence of this in the literature. In addition, since one of the main goals of replacing Pt with PGM-free materials in PEFC is decreasing the cost, reducing the Pt loading on the anode is an interesting approach, especially if this is a non-limiting factor in the performance. Examining again the literature, in the papers reporting the best performances with state of the art PGM-free catalysts in acidic PEFC the Pt loading on the anode is usually in the range of 1.0–0.2 mg cm⁻².^{21,31,33,64–67} Only in one case of high performance MEA the anode loading used was 0.1 mg cm⁻²,¹⁹ and no works report the use of lower loadings. These loadings are much higher than 0.05 mg_{Pt} cm⁻², which is the lower loading considered by Gasteiger et al. for Pt/C MEAs.³⁸ Using an excess of Pt at the anode for an MEA with PGM-free cathode makes sense if the purpose is uniquely to study the cathode performance. This would assure that the anode is not a limiting factor at all. To better clarify the anode loading impact on MEAs with PGM-free cathode, we compared the loading commonly used in the literature 0.2 mg_{Pt} cm⁻², with lower loadings of 0.1 mg_{Pt} cm⁻² and 0.035 mg_{Pt} cm⁻². The latter is even lower than the lower one considered by Gasteiger et al. in their Pt/C MEA study (i.e. 0.05 mg_{Pt} cm⁻²).³⁸

Figures 3a and 3c show the H₂/air polarization curves measured at BOT in cathodic and anodic scan directions for the MEAs prepared with different Pt loadings on the anode (MEAs # 3–4–5 in Table II), and the same cathode loading. The differences are negligible in both the scan directions. This is more clearly depicted in Fig. 3e, where the current density % difference (Δi) between the MEA with the highest Pt loading (0.2 mg cm⁻²) and the two MEAs with lower loadings is shown as a function of the cell potential (E_{cell}). The differences are all below 5% except for the low current density region ($E_{\text{cell}} > 0.6$ V) for the MEA with 0.1 mg_{Pt} cm⁻² in the anodic scan direction, and for the MEA with 0.035 mg_{Pt} cm⁻² in the cathodic scan direction. The observed differences do not follow a monotonic trend with the Pt loading, and thus can be attributable to the experimental error.

The situation is only slightly different for the H₂/O₂ polarization curves in Figs. 3b and 3d. Here, the MEA with 0.035 mg_{Pt} cm⁻² loading performs slightly less than the two MEAs with higher Pt loadings, which are very similar to each other. Figure 3f shows that the Δi is below 5% for the 0.1 mg_{Pt} cm⁻² MEA, and it is still way below 10% also for the 0.035 mg_{Pt} cm⁻² MEA at all E_{cell} values.

The results of this study are beneficial for the community, and clarify that the anode Pt loading can be lowered down to at least 0.035 mg cm⁻² without suffering any relevant performance loss in H₂/air polarization curves compared to the commonly used loadings of 0.2 mg_{Pt} cm⁻² or above, and thus the PEFC cost can be much reduced.

Effects of polarization curve scan direction.—The polarization curve scan direction is a variable that most of the times is not even mentioned in the experimental section of papers, so its influence on the results is not clear. Possibly, many research groups testing the performance of PGM-free catalysts in MEA might have found it to not be impactful, or simply they just decided to use one scan direction instead of the other. Thus, we wanted to clarify this aspect. We measured the polarization curves in voltage control mode, i.e., fixing the voltage and recording the current density for a certain time (75 s) before changing the voltage to the subsequent value. Here, we indicate as “cathodic” the scan direction going from high to low potential values (e.g. from OCV to 0.1 V), which is also sometimes indicated as “negative” scan direction. On the other hand, we

indicate as “anodic” the scan direction going from low to high potential values (e.g. from 0.1 V to OCV), which is also sometimes indicated as “positive” scan direction. The H₂/air polarization curves measured at BOT for the MEAs with different anode catalyst loadings are shown in Fig. 4a–4c. For all the MEAs there is a little difference between the polarization curves measured in cathodic and anodic scan direction. Specifically, the cathodic scan polarization curve seems to provide better performance at low current density, while at high current density (e.g. above 1 A cm⁻² or below 0.3 V) the anodic scan polarization curve provides better performance. Overall, for the two MEAs with higher anode Pt loading the difference between cathodic and anodic scan is lower than for the MEA with 0.035 mg_{Pt} cm⁻². This is valid also for the H₂/O₂ polarization curves shown in Fig. S1a–S1c (available online at stacks.iop.org/JES/168/014503/mmedia).

To minimize the effect of the scan direction when reporting polarization curve data, especially when comparing results obtained by different groups or for different MEAs, a possibility is to report the average of the cathodic and anodic polarization curves. Given the poor stability of many PGM-free catalysts, recording multiple consecutive polarization curves (e.g. three consecutive repeats) in both scan directions could be an interesting strategy to verify the short term stability and obtaining more realistic results, especially for PGM-free catalysts with very high BOT activity, but poor durability.⁶⁸

To apply this method, we measured repeated H₂/air polarization curves in anodic and cathodic direction for 3 times consecutively, for a total of 6 polarization curves (as indicated in Table III). The results are shown in Fig. 4d for the MEA with anode loading of 0.2 mg_{Pt} cm⁻². Then, we averaged the anodic and cathodic polarization curves for the first, second, and third scans separately and all together, and compared the averaged polarization curves with the first polarization curve measured in the cathodic scan direction. From Fig. 4e we can see that the differences are negligible. To better visualize these results, we plotted the Δi as a function of the cell potential in Fig. 4f. For this specific Fe–N–C catalyst, averaging three consecutive cathodic and anodic scans provides a difference below 10% at all potentials compared to the first cathodic scan, denoting a good short-term durability under H₂/air operation. The average of the second scan provides almost the same Δi % difference than the average of all the three scans. The results for the H₂/O₂ polarization curves are shown in Figs. S1d–S1f. In this case, the Δi % difference of the average of all scans lays below 10% only for $E_{\text{cell}} < 0.6$ V (Fig. S1f), denoting a higher catalyst degradation under O₂ rather than under air.

Effects of cathode catalyst loading.—Due to the sluggish ORR kinetics, the PGM-free catalyst loading on the MEA cathode is likely to have a high impact on the performance. To investigate this aspect, we fabricated three MEAs in the same way, but varying the cathode catalyst loading (MEAs # 6–7–8 in Table II). We used 4 mg cm⁻² as a reference loading since this is the value most commonly used in the literature for PGM-free catalysts.¹⁵ Then we chose a lower and a higher value (2 and 6 mg cm⁻²) and compared the respective MEA performances. The MEAs were tested according to the protocol shown in Table IV. Figure 5a depicts the BOT H₂/air polarization curves of the MEAs with the three different cathode catalyst loadings (step 1 in Table IV). The low current density region is better visualized in the semi-logarithmic plot in Fig. 5b. Here, the HFR contribution was subtracted for a fairer comparison since the three MEAs have different HFR values. Overall, the MEA with 4 mg cm⁻² loading seems to provide the best performance vs loading compromise. In fact, the MEA with a lower loading (2 mg cm⁻²) performs worse than the former in the whole potential range. The MEA with a higher loading (6 mg cm⁻²) instead performs slightly better in the low current density region (see also Fig. 5b), showing less than 20 mV improvement at the same current density value up to ca. 0.5 V. Nevertheless, in the high current density region (low voltage), the MEA with 4 mg cm⁻² loading performs better than the

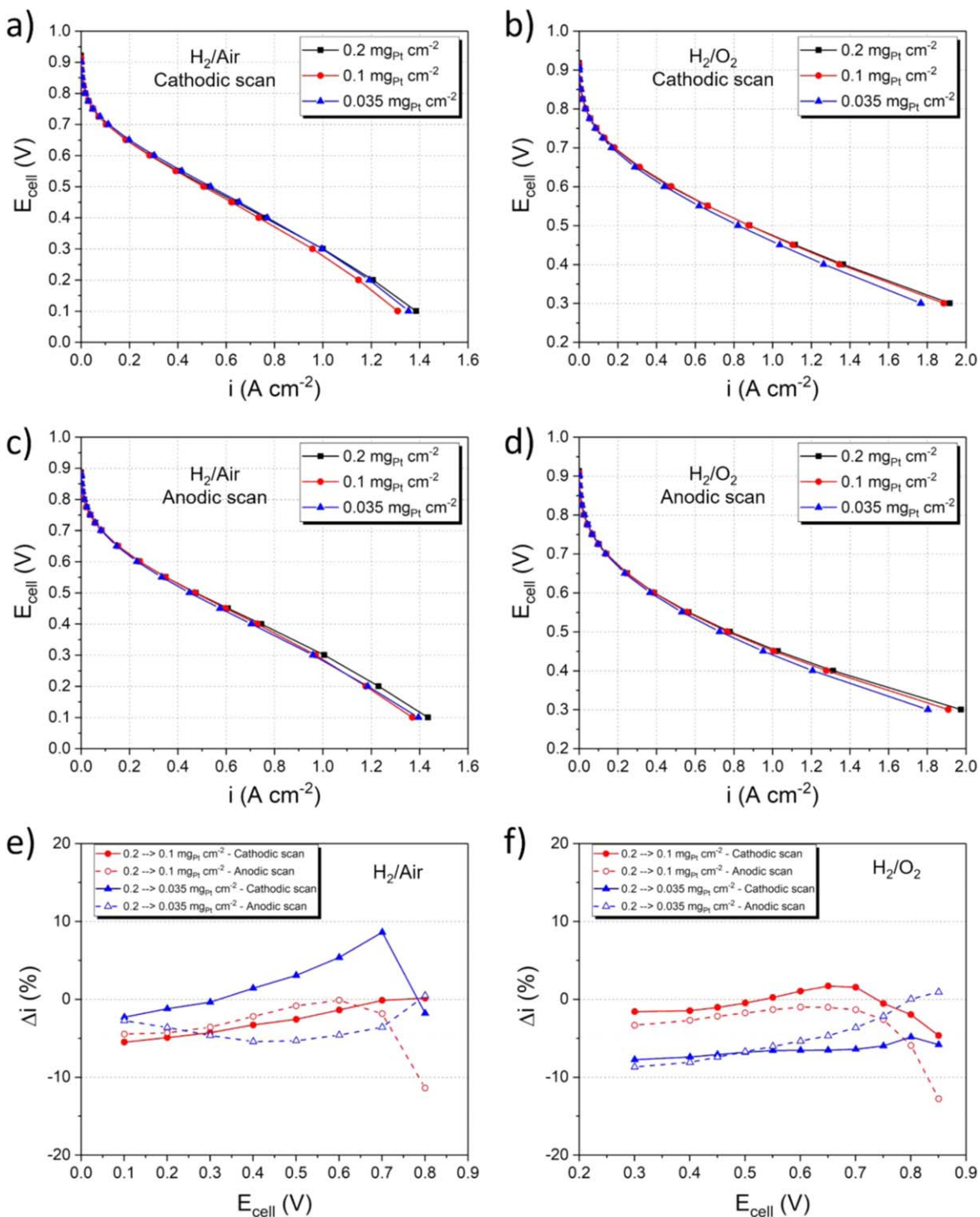


Figure 3. (a)–(d) H₂/air and H₂/O₂ beginning of test polarization curves measured in cathodic and anodic scan directions for the MEAs having different Pt loadings on the anode, and same cathode catalyst loading. (e)–(f) Current density differences (Δi) between the MEAs with reduced anode Pt loadings and the MEA with the highest anode Pt loading of 0.2 mg cm⁻², in function of cell potential. Positive Δi values indicate better performance than the MEA with anode Pt loading of 0.2 mg cm⁻².

6 mg cm⁻² MEA. This is because at high current density the ohmic and mass transport phenomena become the limiting factors. Having a thicker catalyst layer reduces the catalyst utilization due to the higher O₂ and H⁺ transport resistances.²⁹ The H⁺ ions must travel a longer and more tortuous path from the membrane through the ionomer within the CCL to reach all the ORR active sites.^{26,69} At the same time, the O₂ molecular diffusion through the porous structure of CCL is more hindered due to the increased thickness.^{26,30} Hence,

having a high catalyst loading is beneficial only in the low current density (high voltage) region, where the kinetics is the limiting factor. Here, having a higher catalyst loading, and thus more active sites available for the ORR, enables to obtain higher current density. In the high current density region instead, the advantage of more active sites is hidden by the detrimental effects of the H⁺ and O₂ transport resistance increase. If we normalize the HFR-corrected current densities in Fig. 5b by the cathode catalysts loadings, the

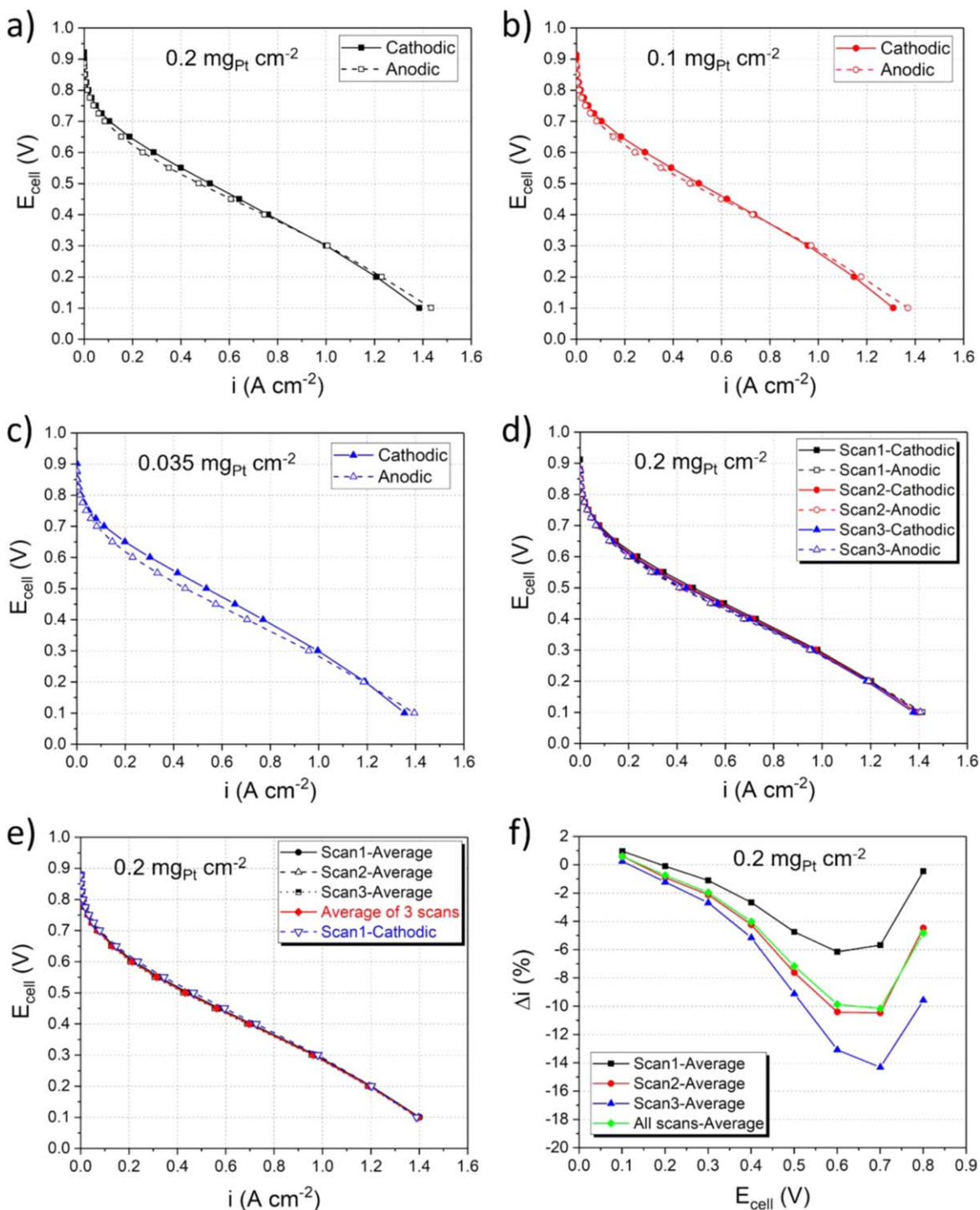


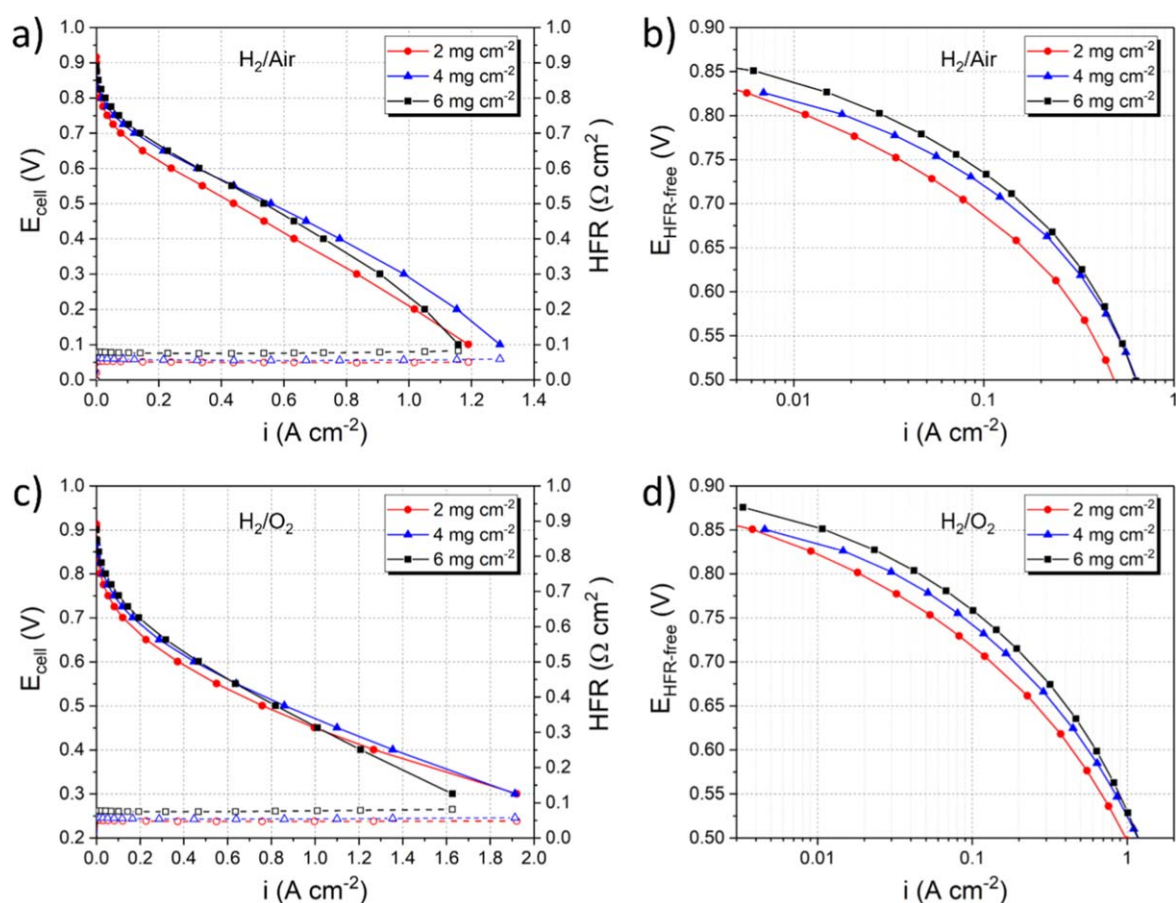
Figure 4. (a)–(c) H₂/air polarization curves measured at beginning of test in cathodic and anodic scan direction for the 3 MEAs fabricated with different anode Pt loadings. (d) The six H₂/air polarization curves measured in 3 consecutive cathodic and anodic scan repeats according to Table III. (e) Average of the cathodic and anodic polarization curves measured in consecutive scans compared with the average of the six polarization curves shown in (d) and the first cathodic polarization curve. (f) Current density difference (Δi) between the average of different scans of cathodic and anodic polarization curves and the first cathodic polarization curve, in function of cell potential. Positive Δi values indicate better performance than the first cathodic polarization curve.

three MEAs show very similar performance, especially in the kinetic region (at low current densities) where the utilization of the catalyst layer is more homogeneous, and does not suffer from contributions of gas phase mass and H⁺ transport losses within the CCL. Otherwise, in the high current density region, the current density normalized for the catalyst loading is higher for the MEAs with lower catalyst loading, due to a better catalyst layer utilization (see Fig. S2a). Figures 5c–5d shows the BOT H₂/O₂ polarization curves

(row 5 of Table IV) for the three MEAs with different cathode catalyst loadings. A similar trend compared to the H₂/air polarization curves was obtained. It is interesting to note that at very high current density (ca. 1.9 A cm⁻²) the MEAs with 2 and 4 mg cm⁻² catalyst loading have the same performance, confirming the high limitations of O₂ gas and H⁺ transport through the thick CCL at high current density. For the MEA with 6 mg cm⁻² loading, the effects of the increased H⁺ and O₂ transport resistance become so high that in the

Table IV. Test protocol for the Series 2 experiments: effect of the PGM-free cathode catalyst loading and gas flow rates. All the polarization curves were measured at 80 °C, 150 kPa, and 100% RH, in the cathodic scan direction.

Order	Type	Flow rate anode/cathode (scm ⁻³ min ⁻¹)	Approx. Stoichiometry at maximum current (anode/cathode)	Notes
1	H ₂ /air	1000/1000	22/9	Control BOT air/baseline
2	H ₂ /air	300/300	8/3	Low flow
3	H ₂ /air	1500/3300	31/27	High flow
4	H ₂ /air	1000/1000	22/9	baseline
5	H ₂ /O ₂	1000/1000	15/30	baseline
6	H ₂ /O ₂	300/300	4.5/9	Low flow
7	H ₂ /O ₂	1500/3300	22/99	High flow
8	H ₂ /O ₂	1000/1000	15/30	baseline
9	H ₂ /air	1000/1000	19/8	Control EOT air

**Figure 5.** (a) Beginning of test H₂/air polarization curves of the three MEAs with different cathode catalyst loadings. (b) HFR-corrected H₂/air polarization curves in the low current density region. (c) H₂/O₂ polarization curves of the three MEAs with different cathode catalyst loadings. (d) HFR-corrected H₂/O₂ polarization curves in the low current density region.

high current density region (above ca. 1 A cm⁻²) the performance is lower than for an MEA with three times lower catalyst loading (2 mg cm⁻²) in both H₂/O₂ and H₂/air polarization curves. The H₂/O₂ polarization curves normalized with respect to the catalyst loading are shown in Fig. S2b, and the results are similar to the H₂/air case.

In Figs. 5a and 5c we also observe that the HFR of the MEAs is higher at higher cathode catalyst loading. This can be due to an increase of the cell electronic resistance due to the increased thickness of the CCLs (ca. 50–100–150 μm for 2–4–6 mg cm⁻² loadings, respectively).

Effects of gas flow rate variation on both anode and cathode simultaneously.—The same MEAs used for the cathode catalyst loading investigation were used to test the effect of the gas flow rates. For all the MEAs of this series, the H₂/air and H₂/O₂ polarization curves were measured in the order shown in Table IV. The flow field geometry and the cell configuration used (see also Fig. 1b) enable to obtain a negligible pressure drop between the beginning of MEA active area and the gas outlet manifold, where the cell pressure is measured.^{30,60} Thus, using this setup, it is possible to operate under “differential cell” conditions, provided that a sufficiently high stoichiometry is used (i.e. sufficiently high gas flow rates are supplied at both electrodes).

The gas flow rate is an important parameter to make sure of being under differential conditions. According to Table IV, we measured polarization curves using three different anode and cathode flow rates. Specifically, the anode (H_2) and cathode (O_2 or air) gas flow rates were varied on both anode and cathode simultaneously. The approximate anode and cathode stoichiometries at the maximum current density measured are also reported in Table IV. The differential FC setup used for the tests in this work has 14 parallel channels, each one with a section area of 0.432 mm^2 , with a total section area of 6.048 mm^2 . The gas flow rates of 300, 100, and $3300 \text{ cm}^3 \text{ min}^{-1}$ result in gas velocities of 0.83, 2.75, and 9.09 m s^{-1} , respectively.

Figures 6a–6e show that the effect of the gas flow rate on the H_2/air polarization curves becomes evident in the high current density region, approximately above ca. 0.6 A cm^{-2} (or below ca. 0.45 V). Increasing the gas flow rates is beneficial in the high current density region, regardless of the cathode catalyst loading. Comparing the three MEAs, for the higher cathode loadings (4 and 6 mg cm^{-2} , Figs. 6c and 6e, respectively), we observe a steeper voltage decrease in the high current density region, more similarly to a “limiting current” condition. This is a signal of gas phase mass transport limitations attributable to the high thickness of the CCL. For these MEAs, an air flow rate increase of 3.3 and 11 times (i.e. from 300 to 1000 and to $3300 \text{ cm}^3 \text{ min}^{-1}$) produces a current density increase at 0.3 V of ca. 0.1 and 0.2 A cm^{-2} , respectively.

For the MEA with low cathode loading (2 mg cm^{-2} , Fig. 6a), the current density decreases more linearly with the voltage, indicating ohmic limitations being more predominant than gas phase mass transport, due to the thinner CCL.

For the H_2/air polarization curves, the performance dependence on the flow rate observed in the high current region is related to the low cathode stoichiometry. With $300 \text{ cm}^3 \text{ min}^{-1}$ air flow rate the cathode stoichiometry at the maximum current is only ca. 3, and the reduced mass transport due to the lower O_2 concentration in air causes additional performance limitations. Increasing the flow rate to $1000 \text{ cm}^3 \text{ min}^{-1}$ increases the stoichiometry to ca. 9, which enables to improve the performance. A further increase of flow rate to $3300 \text{ cm}^3 \text{ min}^{-1}$ brings the stoichiometry up to ca. 27, causing a further performance improvement.

Unlike the H_2/air case, the H_2/O_2 polarization curves (Figs. 6b–6f) do not show any performance dependence on the flow rate in the range examined. With these flow rates, the stoichiometry at the maximum current density is close or way above 10 for the cathode, and below 10 only at $300 \text{ cm}^3 \text{ min}^{-1}$ for the anode (see Table IV). However, as previously demonstrated, the anodic HOR is not limiting at all for these PGM-free cathode MEAs. Thus, even a relatively low anode stoichiometry of ca. 4.5 (at $300 \text{ cm}^3 \text{ min}^{-1}$ flow rate) ensures differential cell operating conditions. These results suggest that for H_2/O_2 operation, gas flow rates of $300 \text{ cm}^3 \text{ min}^{-1}$ on both anode and cathode are enough to provide a sufficiently high stoichiometry to operate under differential conditions in the whole range of current density with this differential cell hardware.

In almost all the polarization curves in Fig. 6, the $1000/1000 \text{ cm}^3 \text{ min}^{-1}$ flow rate show a slightly better performance in the low current density region. This is most likely because these polarization curves were measured first (see order of measurement in Table IV), and a slight catalyst degradation occurred.

Effects of independent gas flow rate variation on anode and cathode.—To investigate more in detail the effect of the gas flow rate variation on the performance, we did an additional set of tests on a new MEA (MEA #9, Table II) in which we varied the gas flow only on one electrode at a time, keeping constant the flow on the other electrode. First, a polarization curve was measured in “standard” conditions, that is, with gas flow rate of $1000 \text{ cm}^3 \text{ min}^{-1}$ on both electrodes. Then, two more polarization curves were measured with a lower and a higher flow rate. Finally, one more polarization curve in the standard conditions was recorded to check

the degradation occurring during the test. This procedure was repeated for both H_2/air and H_2/O_2 polarization curves, first varying the anode flow (keeping constant the cathode flow), and then varying the cathode flow (keeping constant the anode flow), as indicated in Table V.

The results of the anode flow rate variation are shown in Figs. 7a and 7b. An anode flow rate variation from 300 to $2000 \text{ cm}^3 \text{ min}^{-1}$ corresponds to a stoichiometry variation from ca. 6 to ca. 40 at the maximum current density in H_2/air . The same flow rate variation in H_2/O_2 corresponds to a stoichiometry variation from ca. 4 to ca. 30. In either case, no significant performance difference was detected, confirming that the anode flow rate (above $300 \text{ cm}^3 \text{ min}^{-1}$) does not limit the performance of an MEA with PGM-free cathode MEA in the differential cell hardware. Figures 7c and 7d show the impact of the cathode flow rate variation on H_2/air and H_2/O_2 polarization curves, respectively. The flow rate was varied from 300 to $3300 \text{ cm}^3 \text{ min}^{-1}$, causing the stoichiometry to vary from ca. 2.5 to ca. 27 at the maximum current density in H_2/air , and from ca. 9 to ca. 95 in H_2/O_2 polarization curves, respectively.

For the H_2/air case, the impact of the cathode flow rate variation is relevant in the high current density region of the polarization curve (above ca. 0.6 A cm^{-2}), similarly to what described in Section 3.5, where the anode and cathode flow rates were varied concomitantly. These results evidence the importance of appropriately choosing the air flow rate when measuring H_2/air polarization curves with this differential cell hardware.

On the other hand, in H_2/O_2 , the sufficiently high cathode stoichiometry and the enhanced gas phase mass transport due to the use of pure O_2 did not cause any detectable performance difference, even with a more than ten times stoichiometry variation at maximum current density. In each plot in Fig. 7 the difference between the first (BOT) and the last (EOT) polarization curves measured in the “standard” conditions is negligible. However, as shown by Table V, the MEA used for this series of tests (Series 3, MEA#9) was subjected to 16 consecutive polarization curves scans. To better visualize the degradation occurred during this test, Fig. S3 shows the first and last H_2/air polarization curves measured (rows 1 and 16 in Table V).

Conclusions

Several MEA fabrication variables and operating conditions impact the performance of a PEFC with a PGM-free cathode. In this work we have investigated systematically some of these variables using a commercial Fe–N–C catalyst in a differential cell hardware.

- Based on our results, anode catalyst loadings as low as $0.035 \text{ mg}_{\text{Pt}} \text{ cm}^{-2}$ do not limit the H_2/air and H_2/O_2 PEFC performance of PGM-free based MEAs. Even though recommending a specific anode Pt loading is not useful to achieve better performance, fabricating MEAs with PGM-free cathode using an anode loading higher than $0.05 \text{ mg}_{\text{Pt}} \text{ cm}^{-2}$ may simply result in a waste of costly Pt catalyst.
- The polarization curve scan direction in our testing protocol plays a slight role in dictating the performance. Averaging the cathodic (negative sweep) and anodic (positive sweep) polarization curves is a good strategy to mitigate these slight differences. Repeating the cathodic and anodic scan polarization curves for multiple time is also useful to test the short-term stability of the PGM-free catalyst. For the commercial Fe–N–C catalyst used in this work, averaging three consecutive cathodic and anodic polarization curves does not provide a considerable difference compared to measuring just one polarization curve in the cathodic scan direction. However, for a less stable catalyst this might not be true and should be verified.
- The PGM-free catalyst loading on the cathode is an important parameter and must be carefully tuned and specified. For the catalyst and the electrode composition analyzed in this study, a

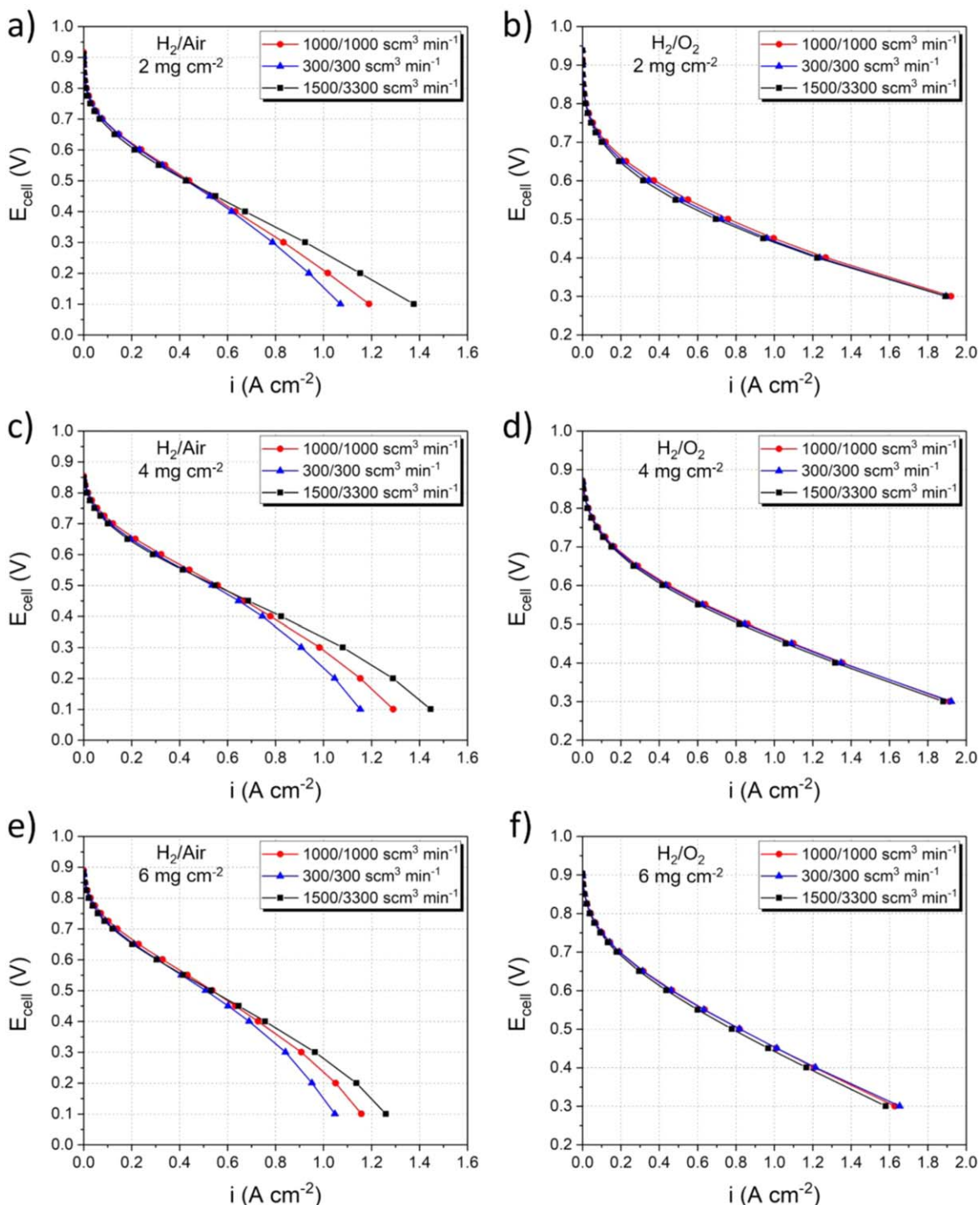


Figure 6. H_2/air and H_2/O_2 polarization curves measured at different gas flow rates (anode/cathode) for the MEAs with different cathode catalyst loading: (a)–(b) 2 mg cm^{-2} ; (c)–(d) 4 mg cm^{-2} ; (e)–(f) 6 mg cm^{-2} .

loading of 4 mg cm^{-2} is the best compromise between activity (number of active sites available) and mass transport properties of the electrode. Higher loadings (e.g. 6 mg cm^{-2}) are not justified because only slight improvement is obtained in the low current density region of the polarization curve, but higher mass transport and ohmic losses in the high current density region are causing considerable performance decays. On the other hand, using a lower loading (e.g. 2 mg cm^{-2}) is not recommendable because a lower performance is obtained.

Thus, a recommendation for the PGM-free cathode catalyst loading could be in the range of 3 to 5 mg cm^{-2} .

- H_2 flow rate variations on the anode between 300 and $2000 \text{ scm}^3 \text{ min}^{-1}$ do not influence the H_2/O_2 and the H_2/Air performance, regardless if the anode flow rate is varied simultaneously or independently from the cathode flow rate.
- For H_2/O_2 polarization curves, O_2 flow rate variations on the cathode in the range 300– $3300 \text{ scm}^3 \text{ min}^{-1}$ do not influence the performance, regardless if the cathode flow rate is varied simultaneously or independently from the anode flow rate.

Table V. Test protocol for the Series 3 experiments: effect of independent anode and cathode gas flow rate variation. All the polarization curves were measured at 80 °C, 150 kPa, and 100% RH, in the cathodic scan direction.

Order	Type	Flow rate anode/cathode (scm ⁻³ min ⁻¹)	Approx. Stoichiometry at maximum current (anode/cathode)	Notes
1	H ₂ /air	1000/1000	20/8	Air Anode variation—baseline
2	H ₂ /air	300/1000	6/8	Air Anode variation—Low flow
3	H ₂ /air	2000/1000	41/8	Air Anode variation—High flow
4	H ₂ /air	1000/1000	20/8	Air Anode variation—baseline
5	H ₂ /O ₂	1000/1000	14/29	O ₂ Anode variation—baseline
6	H ₂ /O ₂	300/1000	4/29	O ₂ Anode variation—Low flow
7	H ₂ /O ₂	2000/1000	29/29	O ₂ Anode variation—High flow
8	H ₂ /O ₂	1000/1000	14/29	O ₂ Anode variation—baseline
9	H ₂ /air	1000/1000	20/8	Air Cathode variation—baseline
10	H ₂ /air	1000/300	20/2.5	Air Cathode variation—Low flow
11	H ₂ /air	1000/3300	20/27	Air Cathode variation—High flow
12	H ₂ /air	1000/1000	20/8	Air Cathode variation—baseline
13	H ₂ /O ₂	1000/1000	14/29	O ₂ Cathode variation—baseline
14	H ₂ /O ₂	1000/300	14/9	O ₂ Cathode variation—Low flow
15	H ₂ /O ₂	1000/3300	14/95	O ₂ Cathode variation—High flow
16	H ₂ /O ₂	1000/1000	14/29	O ₂ cathode variation—baseline

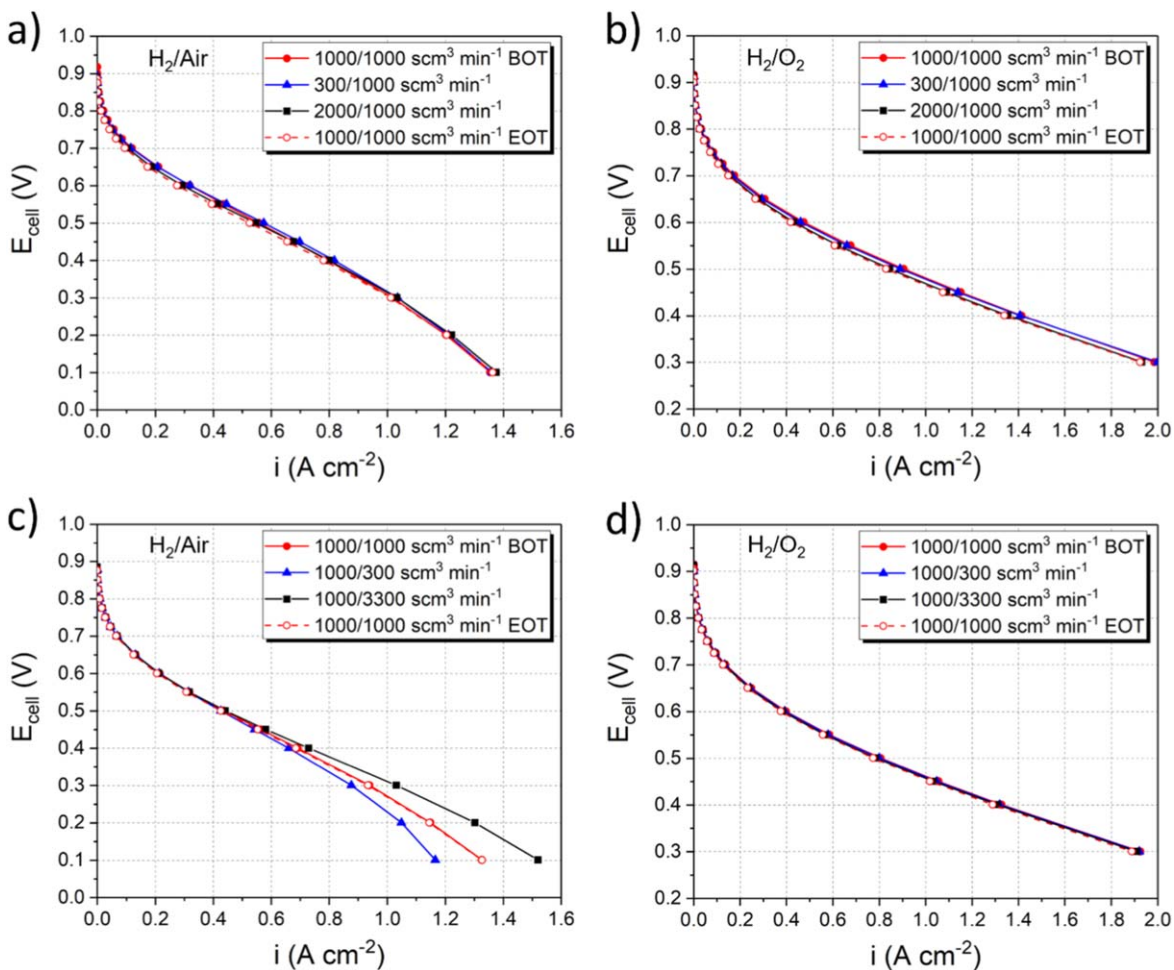


Figure 7. H_2/air and H_2/O_2 polarization curves measured varying independently the gas flow rate on the anode (a)–(b) and on the cathode (c)–(d).

Thus, flow rates $300 \text{ scm}^3 \text{ min}^{-1}$ for both anode and cathode are enough for H_2/O_2 polarization curves measurements using the differential cell hardware. Higher flow rates do not provide any performance improvement and can be considered as a waste of gas.

For H_2/Air polarization curves, the air flow rate on the cathode in the range $300\text{--}3300 \text{ scm}^3 \text{ min}^{-1}$ largely impacts the performance in the high current density region (i.e. above ca. 0.6 A cm^{-2} or below ca. 0.45 V) using the differential cell hardware. Flow rates higher than $1000 \text{ scm}^3 \text{ min}^{-1}$ (i.e. above 8 times the required stoichiometry at the highest current density measured) still provide improvements in the high current density region of the polarization curve. For this reason, the cathode air flow rates must be carefully tuned and clearly specified when measuring H_2/Air polarization curves.

Acknowledgments

This work was authored by Alliance for Sustainable Energy, LLC, the manager and operator of the National Renewable Energy Laboratory for the U.S. Department of Energy (DOE) under Contract No. DE-AC36-08GO28308. Research performed as part of the Electrocatalysis Consortium (ElectroCat), established as part of the Energy Materials Network, which is supported by the U.S. Department of Energy, Office of Energy Efficiency and Renewable Energy, Fuel Cell Technologies Office (FCTO). While we do not endorse any materials presented in this study, Alexey Serov and Barr Zulevi (Pajarito Powder LLC) are gratefully acknowledged for providing the catalysts used in this study. Discussion with Piotr

Zelenay (Los Alamos National Laboratory) and Deborah J. Myers (Argonne National Laboratory) was very valuable. The authors also appreciate the leadership of Dimitrios Papageorgopoulos and Simon Thompson at the FCTO at DOE. The views expressed in the article do not necessarily represent the views of the DOE or the U.S. Government.

ORCID

Luigi Osmieri <https://orcid.org/0000-0002-3111-2270>

Hao Wang <https://orcid.org/0000-0003-0674-0811>

Kenneth C. Neyerlin <https://orcid.org/0000-0002-6753-9698>

References

1. I. EG&G Technical Services, *Fuel Cell Handbook* (U.S. Department of Energy Office of Fossil Energy National Energy Technology Laboratory, Morgantown, WV, USA.) p. 1 (2004). http://osti.gov/energycitations/product.biblio.jsp?osti_id=5616450.
2. (<https://energy.gov/eere/fuelcells/h2scale>)DOE, *Fuel Cell Technologies Office*.
3. S. T. Thompson and D. Papageorgopoulos, *Nat. Catal.*, **2**, 558 (2019).
4. B. G. Pollet, S. S. Kocha, and I. Staffell, *Curr. Opin. Electrochem.*, **16**, 90 (2019).
5. F. C. Cetinbas, X. Wang, R. K. Ahluwalia, N. N. Kariuki, R. P. Winarski, Z. Yiang, J. Sharman, and D. J. Myers, *J. Electrochem. Soc.*, **164**, F1596 (2017).
6. V. Yarlagadda, M. Carpenter, T. E. Moylan, R. S. Kukreja, R. Koestner, W. Gu, L. Thompson, and A. Kongkanand, *ACS Energy Lett.*, **3**, 618 (2018).
7. C. S. Gittleman, A. Kongkanand, D. Masten, and W. Gu, *Curr. Opin. Electrochem.*, **18**, 81 (2019).
8. Y. P. Zhu, C. Guo, Y. Zheng, and S.-Z. Qiao, *Acc. Chem. Res.*, **50**, 915 (2017).
9. F. Jaouen, E. Proietti, M. Lefèvre, R. Chenitz, J.-P. Dodelet, G. Wu, H. T. Chung, C. M. Johnston, and P. Zelenay, *Energy Environ. Sci.*, **4**, 114 (2011).
10. D. Banham and S. Ye, *ACS Energy Lett.*, **2**, 629 (2017).
11. J. Durst, C. Simon, F. Hasche, and H. A. Gasteiger, *J. Electrochem. Soc.*, **162**, F190 (2015).

12. S. T. Thompson, A. R. Wilson, P. Zelenay, D. J. Myers, K. L. More, K. C. Neyerlin, and D. Papageorgopoulos, *Solid State Ionics*, **319**, 68 (2018).
13. U. Martinez, S. Komini Babu, E. F. Holby, H. T. Chung, X. Yin, and P. Zelenay, *Adv. Mater.*, **31**, 1806545 (2019).
14. R. Othman, A. L. Dicks, and Z. Zhu, *Int. J. Hydrogen Energy*, **37**, 357 (2012).
15. L. Osmieri, *ChemEngineering*, **3** (2019).
16. J. Li and F. Jaouen, *Curr. Opin. Electrochem.*, **9**, 198 (2018).
17. M. Chen, Y. He, J. S. Spendelow, and G. Wu, *ACS Energy Lett.*, **4**, 1619 (2019).
18. D. Banham, J.-Y. Choi, T. Kishimoto, and S. Ye, *Adv. Mater.*, **31**, 1804846 (2019).
19. D. Banham, T. Kishimoto, Y. Zhou, T. Sato, K. Bai, J. Ozaki, Y. Imashiro, and S. Ye, *Sci. Adv.*, **4**, 1 (2018).
20. L. Osmieri, S. A. Mauger, M. Ulsh, K. C. Neyerlin, and G. Bender, *J. Power Sources*, **452**, 227829 (2020).
21. R. Chenitz, U. I. Kramm, M. Lefèvre, V. Giblin, G. Zhang, S. Sun, and J.-P. Dodelet, *Energy Environ. Sci.*, **11**, 365–382 (2018).
22. F. Jaouen, D. Jones, N. Coutard, V. Artero, P. Strasser, and A. Kucernak, *Johnson Matthey Technol. Rev.*, **62**, 231 (2018).
23. H. A. Gasteiger, S. S. Kocha, B. Sompalli, and F. T. Wagner, *Appl. Catal. B Environ.*, **56**, 9 (2005).
24. R. K. Ahluwalia, X. Wang, L. Osmieri, J.-K. Peng, H. T. Chung, and K. C. Neyerlin, *J. Electrochem. Soc.*, **166**, F1096 (2019).
25. A. G. Star, G. Wang, S. Medina, S. Pylpenko, and K. C. Neyerlin, *J. Power Sources*, **450**, 227655 (2020).
26. G. Wang, L. Osmieri, A. G. Star, J. Pfeilsticker, and K. C. Neyerlin, *J. Electrochem. Soc.*, **167**, 044519 (2020).
27. S. Komini Babu, H. T. Chung, P. Zelenay, and S. Litster, *ACS Appl. Mater. Interfaces*, **8**, 32764 (2016).
28. U. Beuscher, *J. Electrochem. Soc.*, **153**, A1788 (2006).
29. K. C. Neyerlin, W. Gu, J. Jorne, A. Clark, and H. A. Gasteiger, *J. Electrochem. Soc.*, **154**, B279 (2007).
30. D. R. Baker, D. A. Caulk, K. C. Neyerlin, and M. W. Murphy, *J. Electrochem. Soc.*, **156**, B991 (2009).
31. A. Uddin, L. Dunsmore, H. Zhang, L. Hu, G. Wu, and S. Litster, *ACS Appl. Mater. Interfaces*, **12**, 2216 (2020).
32. J. Li et al., *J. Am. Chem. Soc.*, **142**, 1417 (2020).
33. H. Zhang, H. T. Chung, D. A. Cullen, S. Wagner, U. I. Kramm, K. L. More, P. Zelenay, and G. Wu, *Energy Environ. Sci.*, **12**, 2548 (2019).
34. Y. He et al., *Energy Environ. Sci.*, **12**, 250 (2019).
35. U.S. DRIVE, *Fuel Cell Tech Team Cell Component Accelerated Stress Test and Polarization Curve Protocols for PEM Fuel Cells* (2013), http://energy.gov/sites/prod/files/2015/08/f25/fcto_dwg_usdrive_fctt_accelerated_stress_tests_jan2013.pdf.
36. *Multi-year Research, Development and Demonstration Plan (Fuel Cells section)—Fuel Cell Technologies Office* (DOE Fuel Cell Technologies Office, United States of America) p. 3.4_1 (2016).
37. K. C. Neyerlin, H. A. Gasteiger, C. K. Mittelsteadt, J. Jorne, and W. Gu, *J. Electrochem. Soc.*, **152**, A1073 (2005).
38. H. A. Gasteiger, J. E. Panels, and S. G. Yan, *J. Power Sources*, **127**, 162 (2004).
39. S. Kamarajugadda and S. Mazumder, *J. Power Sources*, **183**, 629 (2008).
40. R. R. Passos, V. A. Paganin, and E. A. Ticianelli, *Electrochim. Acta*, **51**, 5239 (2006).
41. M. Brodt, R. Wycisk, and P. N. Pintauro, *J. Electrochem. Soc.*, **160**, F744 (2013).
42. T. A. Greszler, D. Caulk, and P. Sinha, *J. Electrochem. Soc.*, **159**, F831 (2012).
43. N. P. Subramanian, T. A. Greszler, J. Zhang, W. Gu, and R. Makharia, *J. Electrochem. Soc.*, **159**, B531 (2012).
44. A. Kongkanand and M. F. Mathias, *J. Phys. Chem. Lett.*, **7**, 1127 (2016).
45. F. Jaouen et al., *ACS Appl. Mater. Interfaces*, **1**, 1623 (2009).
46. D. Sebastián, V. Baglio, A. S. Aricò, A. Serov, and P. Atanassov, *Appl. Catal. B Environ.*, **182**, 297 (2015).
47. L. Osmieri, R. Escudero-Cid, A. H. A. Monteverde Videla, P. Ocón, and S. Specchia, *Appl. Catal. B Environ.*, **201**, 253 (2017).
48. C. Lo Vecchio, A. Serov, H. Romero, A. Lubers, B. Zulevi, A. S. Aricò, and V. Baglio, *J. Power Sources*, **437**, 226948 (2019).
49. D. Sebastián, A. Serov, I. Matanovic, K. Aryushkova, P. Atanassov, A. S. Aricò, and V. Baglio, *Nano Energy*, **34**, 195 (2017).
50. U. A. Paulus, T. J. Schmidt, H. A. Gasteiger, and R. J. Behm, *J. Electroanal. Chem.*, **495**, 134 (2001).
51. D. van der Vliet, D. S. Strmcnik, C. Wang, V. R. Stamenkovic, N. M. Markovic, and M. T. M. Koper, *J. Electroanal. Chem.*, **647**, 29 (2010).
52. K. Shinozaki, J. W. Zack, R. M. Richards, B. S. Pivovarov, and S. S. Kocha, *J. Electrochem. Soc.*, **162**, F1144 (2015).
53. B. Wahdame, D. Candusso, and J. M. Kauffmann, *J. Power Sources*, **156**, 92 (2006).
54. J. Ge and H. Liu, *J. Power Sources*, **142**, 56 (2005).
55. G. H. Guvelioglu and H. G. Stenger, *J. Power Sources*, **163**, 882 (2007).
56. Y. Shao, J.-P. Dodelet, G. Wu, and P. Zelenay, *Adv. Mater.*, **31**, 1807615 (2019).
57. U. Martinez, S. Komini Babu, E. F. Holby, and P. Zelenay, *Curr. Opin. Electrochem.*, **9**, 224 (2018).
58. X. Yin et al., *ECS Trans.*, **77**, 1273 (2017).
59. L. Osmieri et al., *Nano Energy*, **75**, 104943 (2020).
60. L. Osmieri et al., *Appl. Catal. B Environ.*, **257**, 117929 (2019).
61. S. Kabir et al., *ACS Appl. Mater. Interfaces*, **11**, 45016 (2019).
62. T. Van Cleve et al., *ACS Appl. Mater. Interfaces*, **11**, 46953 (2019).
63. Y. Li, L. Lin, H. T. Chung, S. Komini Babu, U. Martinez, G. M. Purdy, and P. Zelenay, *ACS Energy Lett.*, **5**, 17261731 (2020).
64. H. T. Chung, D. A. Cullen, D. Higgins, B. T. Sneed, E. F. Holby, K. L. More, and P. Zelenay, *Science*, **357**, 479 (2017).
65. C. Shu, Y. Chen, X.-D. Yang, Y. Liu, S. Chong, Y. Fang, Y. Liu, and W.-H. Yang, *J. Power Sources*, **376**, 161 (2018).
66. J. Shui, C. Chen, L. Grabstanowicz, D. Zhao, and D.-J. Liu, *Proc. Natl. Acad. Sci. U. S. A.*, **112**, 10629 (2015).
67. J. Li et al., *Nat. Catal.*, **1**, 935 (2018).
68. P. Zelenay and D. Myers, *ElectroCat (Electrocatalysis Consortium) DOE Annual Merit Review*. https://hydrogen.energy.gov/pdfs/review20/fc160_myers_zelenay_2020_o.pdf (2020).
69. R. Makharia, M. F. Mathias, and D. R. Baker, *J. Electrochem. Soc.*, **152**, A970A (2005).